

# Measurements of the Cosmological Evolution of Magnetic Fields with the Square Kilometre Array

Martin Krause,<sup>1,2,3\*</sup> Paul Alexander,<sup>1,4</sup> Rosie Bolton,<sup>1</sup> Jörn Geisbüsch,<sup>1</sup>  
David A. Green<sup>1</sup> and Julia Riley<sup>1</sup>

<sup>1</sup>*Astrophysics Group, Cavendish Laboratory, 19 J. J. Thomson Avenue, Cambridge CB3 0HE*

<sup>2</sup>*Max-Planck-Institut für Extraterrestrische Physik, Giessenbachstrasse, 85748 Garching, Germany*

<sup>3</sup>*Universitätssternwarte München, Scheinerstr. 1, 81679 München, Germany*

<sup>4</sup>*Kavli Institute for Cosmology Cambridge, Madingley Road, Cambridge, CB3 0HA*

Accepted 2009 August 5. Received 2009 July 6; in original form 2009 April 3

## ABSTRACT

We investigate the potential of the Square Kilometre Array (SKA) for measuring the magnetic fields in clusters of galaxies via Faraday rotation of background polarised sources. The populations of clusters and radio sources are derived from an analytical cosmological model, combined with an extrapolation of current observational constraints. We adopt an empirical model for the Faraday screen in individual clusters, gauged to observations of nearby clusters and extrapolate the polarisation properties for the radio source population from the NRAO VLA Sky Survey. We find that about 10 per cent of the sky is covered by a significant extragalactic Faraday screen. Most of it has rotation measures between 10 and 100  $\text{rad m}^{-2}$ . We argue that the cluster centres should have up to about 5000  $\text{rad m}^{-2}$ . We show that the proposed mid frequency aperture array of the SKA as well as the lowest band of the SKA dish array are well suited to make measurements for most of these rotation measure values, typically requiring a signal-to-noise of ten. We calculate the spacing of sources forming a grid for the purpose of measuring foreground rotation measures: it reaches a spacing of 36 arcsec for a 100 hour SKA observation per field. We also calculate the statistics for background RM measurements in clusters of galaxies. We find that a first phase of the SKA would allow us to take stacking experiments out to high redshifts ( $> 1$ ), and provide improved magnetic field structure measurements for individual nearby clusters. The full SKA aperture array would be able to make very detailed magnetic field structure measurements of clusters with more than 100 background sources per cluster up to a redshift of 0.5 and more than 1000 background sources per cluster for nearby clusters, and could for reasonable assumptions about future measurements of electron densities in high redshift clusters constrain the power law index for the magnetic field evolution to better than  $\Delta m = 0.4$ , if the magnetic field in clusters should follow  $B \propto (1+z)^m$ .

**Key words:** surveys — cosmology: observations — galaxies: clusters: general — magnetic fields — radio continuum: general — instrumentation: polarimeters

## 1 INTRODUCTION

The plasma between the galaxies in clusters is magnetised. Observations at radio frequencies are our main quantitative probe of cluster magnetic fields. This is done by three main methods: equipartition arguments applied to cluster halo radio sources (e.g. Giovannini et al. 1993), comparison of X-ray Inverse Compton (IC) with the radio synchrotron data in radio sources (e.g. Bagchi et al. 1998), and Faraday rotation of polarised radio sources

within or behind the cluster, combined with X-ray data to determine the electron densities (Kim et al. 1991; Clarke et al. 2001). The results have been reviewed regularly (Carilli & Taylor 2002; Govoni & Feretti 2004; Feretti & Giovannini 2008). Galaxy clusters are found to possess magnetic fields of typically a few, up to of order 10  $\mu\text{G}$ .

The structure within cluster magnetic fields has been deduced from Faraday rotation of extended cluster radio sources (Murgia et al. 2004; Vogt & Enßlin 2005; Govoni et al. 2006; Guidetti et al. 2008). For the few cases observed so far, the data is consistent with a Kolmogorov-type power spectrum. Because the field is frozen into the plasma in the high conductivity limit, the

\* E-mail: M.Krause@mrao.cam.ac.uk, krause@mpe.mpg.de, mkrause@usm.lmu.de

**Table 1.** Comparison of radio telescopes — derived properties.

Name	VLA <sup>a</sup>	SKA AA	SKA Dishes	SKA Dishes Phase 1
$A_{\text{eff}}/T_{\text{sys}}^{\text{b}}$	70–180	10,000	10,000	1,200
frequencies of interest / GHz	0.3–0.34, 1.24–1.7, 4.5–5, 8.1–8.8	0.3–1	0.8–10	0.8–10
instantaneous bandwidth / MHz	86	700	250	250
1-h sensitivity / $\mu\text{Jy}$	17	0.18	0.29	2.5
field of view / square degree <sup>c</sup>	$(0.7/f)^2$	250	2	20 <sup>d</sup>

<sup>a</sup> See: <http://www.vla.nrao.edu/astro/guides/vlas/current/>.

<sup>b</sup> Effective collecting area over system temperature.

<sup>c</sup> For the dish telescopes, given at the bottom of the frequency range;  $f$  denotes the observing frequency in GHz.

<sup>d</sup> Assuming phased array feeds.

structure of the field directly traces the underlying kinematics of the gas.

Current studies of magnetic fields in clusters are limited to a few nearby objects ( $z < 0.1$ ). Hence, we have no means to answer questions regarding the origin and cosmological evolution of these fields. Correspondingly, few cosmological structure formation simulations have included magnetic fields. To date, none have the resolution to address directly the field evolution in galaxy clusters. However, from the eddy turnover times, and the high efficiency of the turbulent dynamo, one might expect that the magnetic energy should always be in equipartition with the turbulent kinetic energy (Ryu, private communication). Hence, studying the cosmological evolution of fields in clusters might not only lead to the origin of magnetism, but also trace cluster kinematics.

Magnetic fields in clusters of galaxies might be connected to the cooling flow problem. If cooling flows in nearby objects are quenched by weak jets, as has been often suggested (e.g. Kaiser & Binney 2003), the magnetic fields will be amplified up to equipartition with the enhanced kinetic energy level provided by the very same jets.

The Faraday rotation method is expected to benefit substantially from new developments of radio telescopes over the coming decade. The Australian ASKAP project, as well as the South African MEERKAT project are expected to start operation within a few years — both instruments will have sensitivities competitive with the eVLA, (enhanced Very Large Array) but with substantially higher survey speed at frequencies below 1.4GHz. The Square Kilometre Array (SKA) is the next generation radio interferometer and will be a transformational instrument with an improvement in sensitivity compared to the eVLA of a factor of fifty with a  $10^5$  increase in survey speed. At frequencies below 500MHz, aperture arrays will form the collector with dishes at frequencies above 1.4 GHz. In the mid frequency range (0.3–1.4 GHz) large survey speeds will be achieved by using aperture arrays or dishes with focal-plane arrays (Schilizzi et al. 2007). Phase 1 of the telescope (with between 10 and 15 percent of the collecting area) is scheduled for operation in about 2015 with phased deployment of the rest of the telescope over the next few years and with completion in 2021/22. Aperture arrays provide the most exciting technology for the mid-frequency range with the largest increase in survey speed provided they can meet an appropriate performance to cost (Alexander & Faulkner 2009). The derived properties for the SKA, based on Schilizzi et al. (2007) and Alexander & Faulkner (2009) are summarised in Table 1, together with a comparison to the VLA.

In this paper, we investigate the potential of these instruments,

in particular the SKA, to measure cosmological evolution in cluster magnetic fields. We concentrate on Faraday rotation studies: the magnetic field along the line of sight rotates the polarisation angle by

$$\Delta\chi = \frac{\text{RM}}{(1+z)^2} \lambda^2, \quad (1)$$

where  $\lambda$  is the observing wavelength and we included the cosmological factor ( $z$  is the redshift of the rotating Faraday screen) to account for the redshift of the radio emission traveling from the Faraday screen to us. This factor ensures that for background sources with redshifts much higher than the targeted cluster, the contribution to the rotation of the polarisation angle from the vicinity of the radio source will be negligible (unless that RM contribution is extremely high), since it occurs at much higher frequencies. RM is related to the thermal electron density,  $n_e$  ( $\text{cm}^{-3}$ ), and the line-of-sight magnetic field,  $B$  ( $\mu\text{G}$ ), as:

$$\text{RM} = 812 \int_0^L n_e B \cdot dl \text{ rad m}^{-2}, \quad (2)$$

where the path-length  $dl$  is measured in kpc.

The rotation measure has contributions from all along the line of sight, from the inter-galactic medium (IGM) in the vicinity of the source itself, from the intra-cluster medium (ICM) in the clusters along the line of sight, and from our own galaxy. The galactic contribution typically dominates at galactic latitudes below about  $|b| < 20^\circ$ . Above  $|b| > 40^\circ$ , the galactic contribution becomes smaller than  $|\text{RM}| < 30 \text{ rad m}^{-2}$  (Simard-Normandin & Kronberg 1980), and can be as small as  $5 \text{ rad m}^{-2}$  (Guidetti et al. 2008). Hence, high rotation measure from extragalactic sources at high galactic latitudes can most likely be attributed to Faraday rotation within the gas in galaxy clusters.

### 1.1 Observations to date

So far, the only individual cluster with a significant number of observed polarised members *and* background sources is the Coma cluster. Seven sources within 35 arcmin display a clearly enhanced  $|\text{RM}|$  between 35 and  $65 \text{ rad m}^{-2}$  (Kim et al. 1990; Feretti et al. 1995). These sources, as well as control sources in the vicinity of the cluster, but avoiding sightlines through Coma’s ICM, have been observed in many individual pointings with the VLA. For the cluster A514, six embedded radio sources have been observed in individual VLA pointings. These show a decline of  $|\text{RM}_{\text{max}}|$  from  $154 \text{ rad m}^{-2}$  in the centre of the cluster to  $15 \text{ rad m}^{-2}$  on

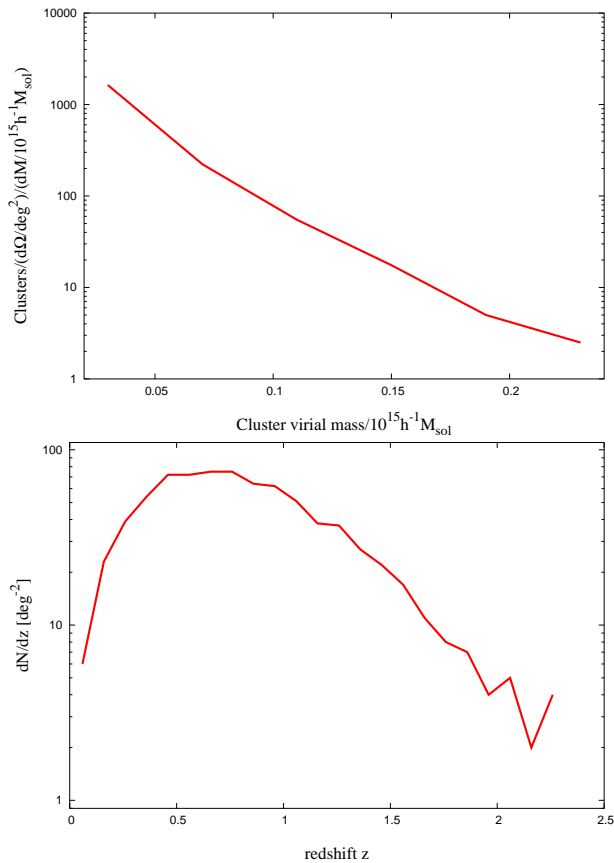


**Figure 1.** Mass (top) and redshift (bottom) distribution of the adopted galaxy cluster model. See text for details of the model.

the outskirts. Several other clusters, each with a few polarised sources, have been observed with similar results (Feretti et al. 1999; Taylor et al. 2001; Govoni et al. 2006; Guidetti et al. 2008). Many clusters have only one or two sufficiently bright radio sources in or behind them<sup>1</sup>. Therefore stacking has been used to infer a general RM value for nearby clusters (Clarke et al. 2001). A systematic increase in  $|\text{RM}|$  is found towards the cluster cores.

First attempts have been made to infer the magnetic field structure via the power-spectrum with Faraday rotation studies. For the cluster A2255, Govoni et al. (2006) measure the Faraday rotation of four embedded radio sources. For different assumptions about the magnetic field power spectrum they can extrapolate this data to predict the synchrotron emission of the radio halo. Comparison to observations of the radio halo then constrains the power law index of the magnetic field’s 3D-power spectrum to the range three to four, consistent with Kolmogorov turbulence, with a possible spatial variation. The model also predicts polarisation of the halo, which is indeed detected.

This paper is structured as follows: First, we discuss the simulation method in Section 2. The Faraday rotation detection statistics and the implications for the measurement of the cosmological evolution of the magnetic field in clusters are presented in Section 3. We discuss our findings in Section 4, and summarize them in Section 5. Throughout, we use the following cosmological parameters:  $h = 0.7$ ,  $\Omega_m = 0.3$ ,  $\Omega_\Lambda = 0.7$ .

<sup>1</sup> See: <http://www.mpa-garching.mpg.de/~kdolag/BCluster/>.

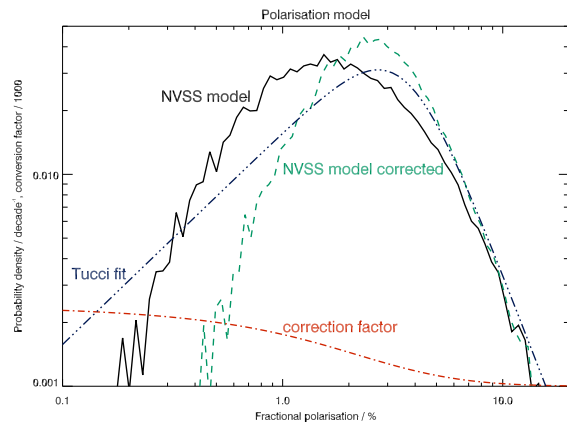


**Figure 2.** Distribution of the fractional polarisation for the radio source model. The dark blue triple dot-dashed line represents the fit from Tucci et al. (2003) (not yet corrected for Faraday depolarisation). The solid black line represents our adaptation of this fit. This model is corrected for Faraday depolarisation by the polarisation dependent correction factor shown as red dot-dashed curve (divided by 1000). The model finally adopted in this paper is shown as a green dashed line. The polarisation distribution functions agree all at high fractional polarisations, where they are gauged against NVSS data.

## 2 THE SIMULATIONS

In order to assess the effect of cluster Faraday screens on the polarisation of background radio sources, a relatively sophisticated model of clusters and source populations is required.

### 2.1 Cluster model

In order to model the cluster number within an observed patch of sky (here  $10 \text{ deg}^2$ ), we require a model for the cosmologically evolving cluster mass function. For this, we employ a cluster mass function whose multiplicity function (see e.g. Sheth & Tormen 1999) is based on a moving barrier shape ansatz and depends on a minimal number of parameters to provide a suitable fit to numerical simulations. In particular, the shape of the used mass function has been derived from N-body simulations of large cosmological volumes and high resolutions following the method described in Jenkins et al. (2001). The above model gives the cluster mass function as a function of redshift. We adopt a lower mass cutoff of  $3 \times 10^{13} M_\odot$  and for a given realisation of the sky model derive cluster counts as a function of redshift, making allowance for cosmic variance. Our resulting galaxy cluster catalogue contains 775 objects, with redshifts up to  $\sim 2.3$ . The properties of our generated galaxy cluster sample are illustrated in Fig. 1.

In our model, clusters are distributed randomly and radio sources are either background or foreground objects with respect to a given cluster. Every object is placed on a 3D grid, covering  $\sqrt{10} \times \sqrt{10}$  square degree and the redshift space from zero to eight. The spatial resolution is  $6000 \times 6000$  cells, and redshift space is covered by 240 cells. This gives an effective resolution of 1.9 arcsec and  $dz = 0.033$  in the third dimension.

### 2.2 Rotation measure model

The observational data on the structure of magnetic fields in clusters is currently sparse. Based on Clarke et al. (2001), we therefore employ a simple model for the rotation measure, with a peak value

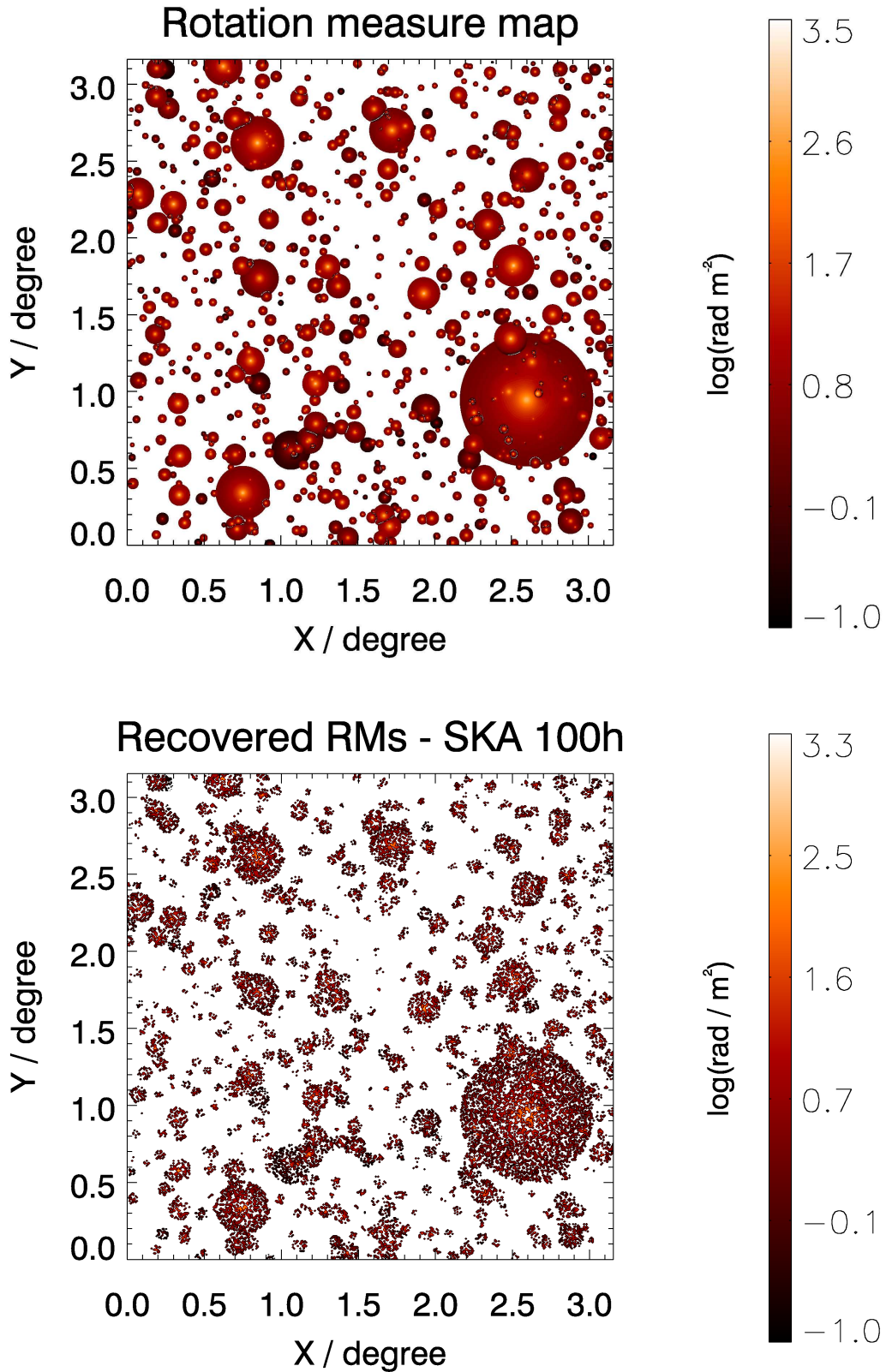


**Figure 3.** Top: Derived distribution of cosmological rotation measures on the sky due to galaxy clusters. Bottom: Recovered RM-sky due to background radio sources for a 100 h SKA-AA observation. To enhance contrast, the resolution has been reduced by a factor of ten compared to the figure on the top. The real field of view as planned to date would be 25 times larger.

(justified in Section 2.9 below) drawn from a uniform random distribution between  $RM_0 = \pm 5000 \text{ rad m}^{-2}$ , and a decline according to a  $\beta$ -model:

$$RM(r) = RM_0(1 + r^2/r_0^2)^{-3\beta_{RM}/2}. \quad (3)$$

We use  $\beta_{RM} = 1$  (see below) and  $r_0 = 0.0636 r_{200}$  (Biviano & Salucci 2006), where  $r_{200}$  is the radius within which there is an over-density of a factor 200 compared to the mean density of the universe at the redshift of the cluster.  $r_{200}$  is roughly equal to the virial radius of the cluster. This results in core radii between 20 and 110 kpc, which corresponds to angular sizes between a few arcseconds to half an arcminute.

Biviano & Salucci (2006) give a value of  $\beta = 2/3$  for the gas density distribution in clusters of galaxies. The temperature distribution in clusters of galaxies is typically not far from isothermal (except in the centres of cool core clusters). Therefore, the pressure follows a very similar radial profile as that of the density. Equipartition between the magnetic and the thermal pressure is probably a reasonable assumption for the magnetic field distribution in clusters, and consistent with some RM-data (e.g. Govoni et al. 2006; Guidetti et al. 2008). Consequently, we adopt a value of  $\beta_m = 1/3$  for the radial distribution of the magnetic field strength along the line-of-sight. The line-of-sight integral then results in the  $\beta$ -model for the rotation measure described in equation (3) above, with  $\beta_{RM} = 1$ . We calculate the rotation measure contribution out to the virial radius.

We show in Fig. 3 (top) the resulting distribution of rotation measures due to the simulated galaxy clusters. Much of the sky is covered with galaxy clusters, however, many of the systems have small rotation measures. About 12 per cent of the sky is covered with regions of at least  $10 \text{ rad m}^{-2}$ . The fraction reduces by a factor of about two if one considers rotation measures above  $20 \text{ rad m}^{-2}$ . In our chosen cosmology, only 34 per cent of all clusters are located beyond a redshift of one. These are obviously smaller on average than the lower redshift population. Hence, essentially all of the area coverage happens up to a redshift of unity (Fig. 4). Therefore, up to this redshift, structure determination should be much easier than beyond.

### 2.3 Radio source model

To obtain realistic models of the radio source populations, we use the publically available SKADS (Square Kilometre Array European Design Study) synthetic radio source catalogue (*SKADS simulated skies*,  $S^3$ ; Wilman et al. 2008<sup>2</sup>). The catalogue is derived from semi-empirical simulations of different populations of radio continuum sources and extends down to faint flux limits in order to allow observation simulations of high-sensitive future radio telescopes, such as the SKA. The source populations included in the catalogue are radio-loud (FR I and FR II) and radio-quiet AGNs as well as radio emitting starburst and normal disk galaxies. The luminosity function corresponding to each class of sources is derived empirically from available observations. The fits are extrapolated to low luminosities and assume redshift evolutions to assure the simulations are complete down to the instrumentally expected (faint) flux limits. Our version of the catalogue covers ten square degrees of sky out to a redshift of eight with a 1.4 GHz flux limit of  $1 \mu\text{Jy}$  in Stokes  $I$ . See Wilman et al. (2008) for a detailed description of the radio source simulations.

<sup>2</sup> See: <http://s-cubed.physics.ox.ac.uk/>.

### 2.4 Polarisation model

The degree of polarisation has to be determined for individual sources. We base our prediction of the polarisation of these radio sources on the statistics of the NRAO VLA Sky Survey (NVSS) catalogue (Condon et al. 1998). Tucci et al. (2003) have analysed polarisation statistics from the NVSS and other sources in detail. Depending on spectral shape and source flux, they derive median fractional polarisations between 1.12 and 1.77 per cent for NVSS sources. For the NVSS (1.4 GHz), the probability distribution of the fractional polarisation declines monotonically, but for higher observing frequencies, a turnover may be seen towards lower fractional polarisation. This is due to a systematic increase of the fractional polarisation with observing frequency. Tucci et al. (2003) explain these findings by Faraday depolarisation. Therefore, we expect that the low frequency distribution function also turns over at a not yet measured fractional polarisation. We therefore fit a log-normal function to the measured part of the fractional polarisation distribution function at 1.4 GHz. This results in a median value of 1.64 per cent and a standard deviation of 0.7 per cent. Tucci et al. (2003) believe that some of the NVSS sources are depolarised by differential Faraday rotation in intervening galaxy clusters. We argue that this would be much less so for SKA observations: The main reason is that with lower flux limit the radio source population changes. Extended jet sources dominate at high flux densities, and star forming galaxies at increasing distance and decreasing angular size at lower flux densities. For high redshift galaxy clusters, the depolarisation frequency is reduced by a factor  $(1+z)^{-1}$ . Extended sources behind nearby clusters will be much better resolved than by the NVSS (45 arcsec). For a turbulent power spectrum, the RM variations should have less power on smaller scales, hence the depolarisation frequency will be lower (Krause et al. 2007).

For these reasons, we adopt the de-depolarisation model from Tucci et al. (2003) to derive the intrinsic polarisation  $\Pi$  from the potentially Faraday depolarised polarisation  $\Pi_{FD}$ , that is drawn from a random distribution as described above:

$$\begin{aligned} \Pi &= \Pi_{FD} f(\Pi_{FD}, \nu_{\text{GHz}}) / f(\Pi_{FD}, 1.4) \\ f(p, \nu) &= 72 \log(0.5\nu^{0.4} + 0.75) \exp(-3.2p^{0.35} + 0.8). \end{aligned} \quad (4)$$

Here,  $\nu_{\text{GHz}}$  is a reference frequency in GHz. We use 10 GHz as the reference frequency, assuming that Faraday depolarisation for NVSS sources mainly occurs below 10 GHz. The correction increases the fractional polarisation by a factor of about two, for those sources with low polarisation at 1.4 GHz, as shown in Fig. 2. This effect has been measured already: Taylor et al. (2007) measure an increase of the fractional polarisation downwards of 100 mJy of a factor of three compared to the high flux density sources, in agreement with the model we propose.

### 2.5 Redshift distribution

For decreasing flux limit, the radio source counts are dominated by sources of increasing redshift. We show the redshift distribution for different (polarised) flux limited samples in Fig. 5. For a polarised flux-density of  $100 \mu\text{Jy}$ , roughly the level of current studies (Taylor et al. 2007), the median redshift is 0.6. It rises to 1.3 for a polarised flux limit of  $0.1 \mu\text{Jy}$ , appropriate for a 100 h SKA observation. Even for the highest redshifts, we still predict thousands of background sources per square degree for this flux limit.

## 2.6 Required signal-to-noise for RM measurements

A distinctive feature of the next generation of radio telescopes is that a large bandwidth and high spectral resolution will be available simultaneously. Rotation measure synthesis is an established technique to analyse RM data. However, for the analysis of the RM-grid, we wish to extract information from the faintest detectable sources. For the faintest sources we will extract a single value of the rotation measure. Here, we consider the minimum signal-to-noise on a point source required for this. Faraday rotation leads to sinusoidal variation with respect to  $\lambda^2$  across the band for the Stokes parameters  $Q$  and  $U$ , modulated by a function giving the fractional polarisation as a function of wavelength and the intrinsic spectrum of the source. We consider normalised Stokes parameters:

$$\begin{aligned} \begin{pmatrix} Q' \\ U' \end{pmatrix} &= (Q^2 + U^2)^{-1/2} \begin{pmatrix} Q \\ U \end{pmatrix} \\ &= \begin{pmatrix} \cos(2PA + 2RM\lambda^2) \\ \sin(2PA + 2RM\lambda^2) \end{pmatrix}, \end{aligned} \quad (5)$$

where  $Q$  and  $U$  are the ordinary Stokes parameters. To assess the required signal-to-noise ratio (SNR), required of a background source to measure a given foreground RM, we perform Monte-Carlo simulations. Our simulated data were for a background source with a spectral index of 0.7 – we simulate the observing band, taking a constant channel width of  $\Delta\nu = 1$  MHz. We perform a combined  $\chi^2$ -fit to the normalised Stokes parameters, and use the flux at 1.4 GHz as a reference point for the SNR. For infinite SNR, the minimisation of  $\chi^2$  would be straight forward. For decreasing SNR, additional minima appear in  $\chi^2$  as a function of RM. For a SNR of 10 (100) the distance between these minima is of order 1 rad m<sup>-2</sup> (100 rad m<sup>-2</sup>). A dense grid of starting guesses is therefore essential, for a gradient search method to find the global minimum. The actual values of  $\chi^2$  differ only by a few percent, with the exception of the  $\chi^2$  for the true RM, and its negative. We find that  $\chi^2$  for the true RM and its negative, are significantly lower than all other RMs (five times the standard deviation for 400 starting guesses) for a signal to noise of four and higher.

The sign ambiguity is due to the symmetry properties of the trigonometric functions. If a set (PA, RM), where PA is the high frequency polarisation angle (compare equation (5)), are the correct parameters to describe both functions,  $Q'$ (PA, RM) and  $U'$ (PA, RM), then  $(\pi + PA, -RM)$  will be another solution regarding  $Q'$  and  $(-PA, -RM)$  respectively for  $U'$ :

$$\begin{aligned} Q'(\text{PA}, \text{RM}) &= Q'(\pi + \text{PA}, -\text{RM}) \\ U'(\text{PA}, \text{RM}) &= U'(-\text{PA}, -\text{RM}) \end{aligned}$$

To fix the sign at low SNR, for each set of fitted parameters for  $Q'$  we also performed two fits for  $U'$  with starting guesses of  $(\pi - \text{PA}, \text{RM})$  and  $(\text{PA}, \text{RM})$ , respectively, allowing only RM to vary, i.e. keeping the high frequency polarisation angle fixed. If the fit with  $(\text{PA}, \text{RM})$  leads to the lowest minimum of  $\chi^2$ , then we have found the correct RM. However, if the fit with  $(\pi - \text{PA}, \text{RM})$  produces the lowest minimum of  $\chi^2$ , then  $-\text{RM}$  will be the correct rotation measure. The procedure is then repeated with  $U'$  and  $Q'$  exchanged. We may thus produce a combined  $\chi^2$  for RM and  $-\text{RM}$ . Selecting on the combined  $\chi^2$ , we are able to recover the correct sign.

For RMs between 3 and 3000 rad m<sup>-2</sup>, we find a minimum SNR between four and ten. This is true for the observing bands from 800 MHz to 1050 MHz as well as 300 MHz to 1000 MHz. In the following, we assume that a RM measurement may be done for any source detected at an SNR of ten in polarised flux.

## 2.7 Rotation measure grid

For observations of nearby clusters, as well as the galaxy, it is useful to compute the root-area-average distance between polarised background sources. Fig. 6 shows the average grid spacing over observing time for the adopted SKA and SKA phase 1 sensitivities. We use the point source sensitivity limit according to Wrobel & Walker (1999):

$$ds = \frac{k_B T_{\text{sys}}}{\sqrt{2} d\nu \tau A \epsilon}, \quad (6)$$

where,  $k_B$  is Boltzmann's constant,  $T_{\text{sys}}$  is the telescope's system temperature,  $A$  the total effective area,  $d\nu$  the bandwidth,  $\tau$  the observing time and  $\epsilon$  the overall efficiency. Adopting a SNR of ten, we count the sources above the sensitivity limit for a particular telescope and observing time. The total source counts are roughly inversely proportional to the polarised flux, which is an effect of the adding up of the contributions from different source types. So, while the galaxies constitute the majority of the sources at low fluxes, other source types still contribute enough to flatten the overall distribution considerably.

## 2.8 Expected RM values

For each background source, we calculate the observed rotation measure by integrating through the simulation volume from the observed source to the observer. We show the cumulative histogram of all the rotation measures produced in this way in Fig. 7. We find that the majority of rotation measures are in the range 10–100 rad m<sup>-2</sup>, due to the fact that most of the area comes from the outskirts of the clusters. The highest rotation measures come of course from the cluster centres. For a given frequency band and rotation measure range, a particular SNR is required. As shown above in Section 2.6, both of the frequency ranges, 300 MHz to 1000 MHz (aperture array) and 800 MHz to 1050 MHz (dish array), should be suitable for the great majority of expected rotation measures.

## 2.9 Core rotation measures

For each radio source within three virial radii of a given cluster centre, we also calculate the respective impact parameter, i.e. the projected distance to the cluster centre. We show these rotation measures against the impact parameter, for low redshift ( $z < 0.5$ ), high mass ( $M > 10^{14} M_\odot$ ) clusters and a polarised flux limit of 1  $\mu\text{Jy}$  in Fig. 8. These cuts were employed in Clarke et al. (2001), and their data is also shown in Fig. 8. But our model and the observational data show only RM values up to  $|\text{RM}| < 300$  rad m<sup>-2</sup>, whereas our model has peak values of 5000 rad m<sup>-2</sup> in the cluster centres. The reason is that at the high flux cut adopted here, the RM-grid is still very sparse, and hardly any source is located within the core radius. If we employ a lower central RM, with the same cuts, the simulated RM spread on the scale of the virial radius would be too small compared to the observed data. As can be seen, the central rotation measures of about 5000 rad m<sup>-2</sup> that are used in the simulated data here are necessary to reproduce the observed spread of rotation measures. For distances greater than 1000 kpc and random sightlines, we encounter high RMs from neighbouring clusters. These are not present in Clarke et al. (2001), as they select their control sample avoiding known X-ray clusters.

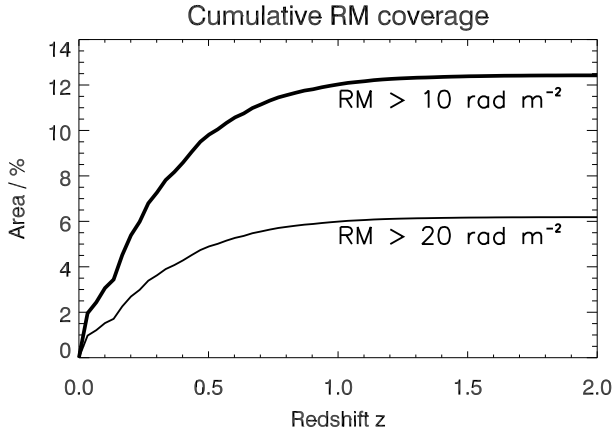


**Figure 4.** Fraction of sky covered with  $RM > 10 \text{ rad m}^{-2}$  (upper curve) and  $RM > 20 \text{ rad m}^{-2}$  (lower curve).

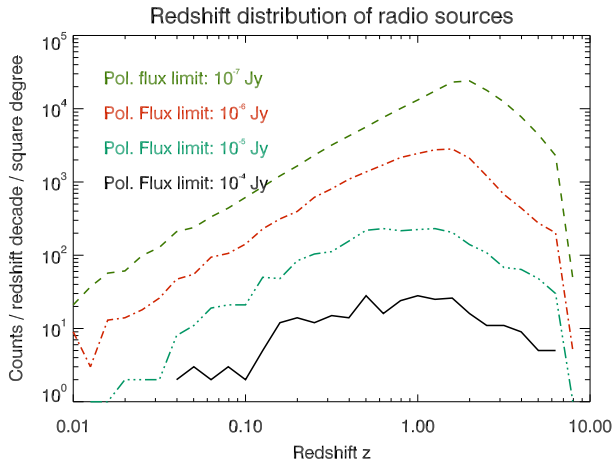


**Figure 5.** Distribution of radio sources against redshift for different polarised flux limits. From top to bottom, the curves represent: 0.1, 1, 10, and 100  $\mu\text{Jy}$ . The median redshift is 0.6, 0.6, 0.8, and 1.3.

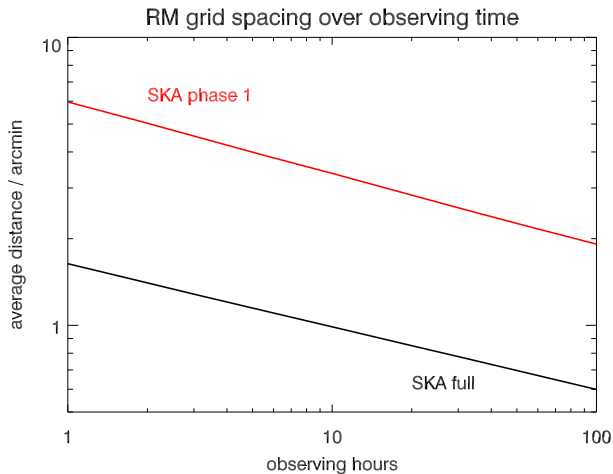


**Figure 6.** RM-grid spacing for different telescopes and a SNR of ten.

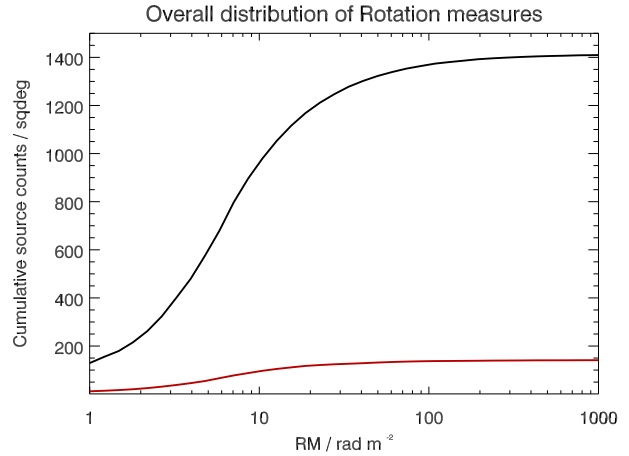


**Figure 7.** Cumulative histogram of all the rotation measures we expect to find within one square degree for a polarised flux limit of 1  $\mu\text{Jy}$  (lower red curve) and 0.1  $\mu\text{Jy}$  (upper black curve). In any case, we expect most of the measurements to yield rotation measures of order 10 to one hundred  $\text{rad m}^{-2}$ .

### 3 RESULTS

#### 3.1 Detection statistics

We show the detection statistics for the SKA aperture array and the phase 1 SKA in Fig. 10 and Table 2. The histograms demonstrate the progress that can be expected from the SKA, especially the full aperture array.

For a one hour phase 1 dish blind survey, we predict to find 30, 214, and 148 clusters in the redshift ranges 0–0.2, 0.2–0.5, 0.5–1, respectively, with more than one background RM measurement, each. We also predict a few detections at higher redshift. This would allow stacking experiments for different redshift bins out to a redshift of at least one. Also, one could determine the decline of the average RM with cluster radius better than presently possible. This could answer the question whether the magnetic field energy density follows the thermal energy density. We also would have some chance to find about a couple of nearby clusters with 30–100 RMs, allowing an improved determination of the field structure. 30 background sources should be enough to constrain the power spectrum (Govoni et al. 2006; Guidetti et al. 2008). Since the positions of the big nearby clusters are known, a targeted survey would certainly yield about this number of RMs.

A 100 hour phase 1 observation would result in 26 clusters at  $z < 0.5$  with more than 30 background sources, and a couple of these having more than 300 background sources. This would allow to study the field structure in some detail. Up to a redshift of unity, nearly every cluster in the field of view should have at least one background source. Even beyond  $z = 1$ , we predict to find 490 clusters with one to several background sources. This would allow the extension of the stacking method to this redshift.

The full SKA aperture array will finally allow to measure the structure of the magnetic field in great detail: Even for a 1 hour observation, each low redshift cluster will at least have 10 background sources 25 of which over three hundred. We predict to find 325 clusters in total with more than 30 background sources, distributed over a redshift range up to 0.5, promising good statistics of the variance of the power spectrum from cluster to cluster. More than 10,000 clusters would be detected with at least one RM measurement beyond a redshift of 0.5.

For a 100 hour pointing, we will be able to constrain the power

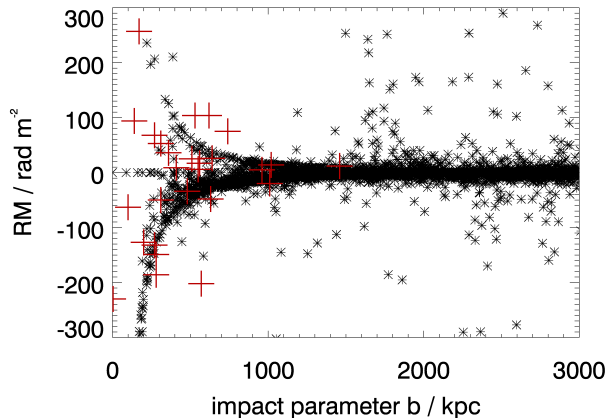


**Figure 8.** Rotation measure against impact parameter. The impact parameter is the projected distance of a radio source to a given cluster centre. Low redshift ( $z < 0.5$ ), high mass ( $M > 10^{14} M_{\odot}$ ) clusters have been selected in order to compare to the observed data of Clarke et al. (2001). The polarised flux limit is  $1 \mu\text{Jy}$ , as in Clarke et al. (2001). Observational data from Clarke et al. (2001) (cluster sample only) is provided as red crosses. For distances greater than 1000 kpc, the sightlines to the radio sources pierce neighbouring clusters. To get the observed RM spread at the observed impact parameters, central RMs of about  $5000 \text{ rad m}^{-2}$  are necessary.

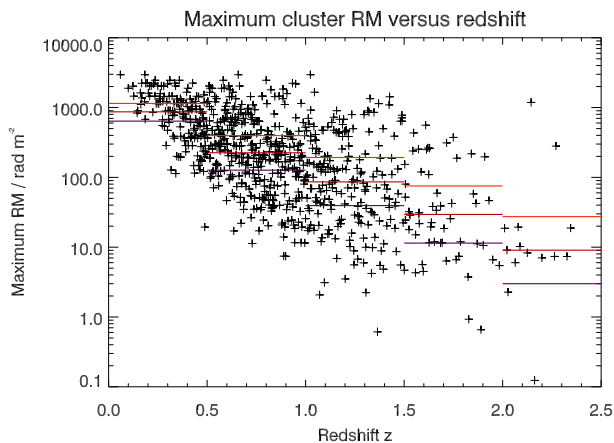


**Figure 9.** Maximum rotation measure seen against any given cluster in our sample against cluster redshift for a polarised flux limit of  $0.1 \mu\text{Jy}$ . The red lines denote the median for sub-samples with corresponding redshifts (0–0.5, 0.5–1, 1–1.5, 1.5–2,  $> 2$ ). The purple lines denote the measured rotation measures if the true rotation measures would decline with redshift as  $(1+z)^{-1}$ , the orange line displays the medians for an increase proportional to  $(1+z)$ .

spectrum for many clusters in the field of view up to a redshift of one ( $> 5,000$  clusters with more than 30 background sources). Up to a redshift of one, we expect  $> 1,000$  clusters with at least 100 RMs. Only for such clusters, we may expect to *resolve* the core in some cases, i.e. to have at least one background source within the cluster’s core radius. A 100 hour pointing would correspond roughly to the sensitivity limit used in Fig. 9, where we show the decrease of the maximum rotation measure in any given cluster with redshift due to the decreased likelihood to get a background source within the core radius. 25 clusters should have more than 1000 background sources, and hence allow a very detailed determination of the magnetic field structure, even in the cluster cores. Due to the limited field of view, the full SKA dish array would

not nearly reach the detection rates of the aperture array. Even a 100 hour blind survey would only yield 24 clusters with more than 30 background sources.

### 3.2 Cosmological evolution

Clusters at higher redshift cover less area of sky (up to a redshift of 1.6). Also, there are fewer sources behind a unit area at higher redshift. Therefore, the probability that a cluster centre has a background object decreases as the redshift increases. We plot the maximum rotation measure that we detect for a polarised flux limit of  $0.1 \mu\text{Jy}$  against any given cluster versus the cluster redshift in Fig. 9. Out to a redshift of unity, there is still a good chance of finding sightlines through the cluster core. However, the median maximum rotation measure decreases by almost a factor of four for clusters with redshift 0.5–1 compared to ones at 0–0.5. The decrease in the median of the measured maximum rotation measure is almost exponential with redshift, with an  $1/e$ -decay length in  $z$  close to 0.4. We can check the detectability of possible trends with redshift by multiplying the rotation measures with  $(1+z)^n$  where we have chosen  $n$  to be  $\pm 1$  as example. The change in the median rotation measure is also indicated in Fig. 9. The decay length changes to 0.3 and 0.5, respectively. If we compare the redshift intervals 0–0.5 and 0.5–1, we predict a decrease of the median rotation measure by factors of about 3, 4 and 5, respectively (compare with Table 3, which is normalised to the low redshift value).

The statistical error on the median maximum rotation measure is given by:

$$\sigma_M = 1.253\sigma/\sqrt{N},$$

where  $\sigma$  is the standard deviation and  $N$  is the number of sources in the respective bin. We have calculated the median maximum RM for any given cluster and the statistical errors for a 100 h SKA AA observation for different values of  $n$ . This is shown in Table 3. Differences in the exponent  $n$  of 0.3 could be distinguished.

## 4 DISCUSSION

We assess the capability of the SKA and its precursor, phase 1 SKA, to detect rotation measures and determine the evolution of magnetic fields in galaxy clusters. Our cluster and radio source simulations are based on standard cosmological methods and extrapolation of available observational data. We use a fractional polarisation model based on NVSS data, moderately corrected for Faraday depolarisation, at low fractional polarisations, only.

We find that about 10 per cent of the whole sky should be covered with rotation measures greater than  $10 \text{ rad m}^{-2}$ . If the cosmology is known, this may serve as an additional constraint to check for the proper removal of the Milky Way’s RM foreground. Large clusters can have a RM contribution from background clusters. However, the contamination occurs mainly on the outskirts of these clusters.

Our simulations show that core RMs of about  $5000 \text{ rad m}^{-2}$  are necessary to explain the currently known stacking data, which shows about  $200 \text{ rad m}^{-2}$  on the scale of the virial radius. RMs against central cluster radio sources often reach values comparable to our core RMs (Carilli & Taylor 2002). This suggests that our assumption for the core RMs is realistic, but also that the functional form of the radial decline we assume is not too far from reality.

How would the derived statistics change if one were to change the radial RM-profile? The adopted profile has high core values



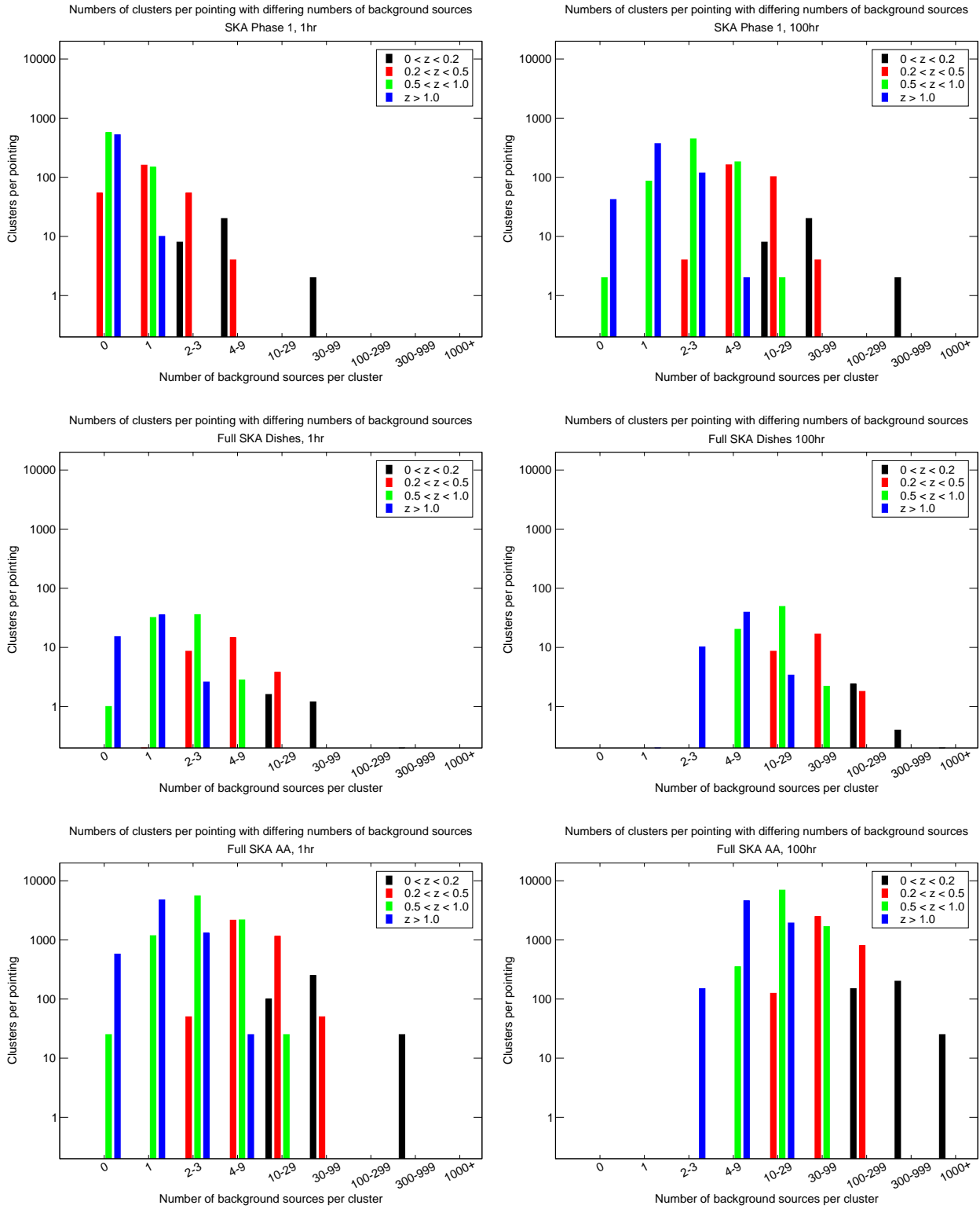


**Figure 10.** Detection statistics for the SKA aperture array (bottom row), the full SKA dish array (middle row) and the phase 1 SKA dish array (top row), telescope specs from Table 1, for an observing time of 1 hour (left) and 100 hours (right), respectively. We plot the number of background sources per cluster on the horizontal axis, and the cluster counts for the particular bins on the vertical axis. The huge number counts found with the full SKA aperture array is a merit of its huge field of view (250 square degrees) combined with its high sensitivity. The same information is provided in tabular form in Table 2.

**Table 2.** Cluster counts with a given number of background sources.

Redshift interval	Number of polarised background sources per cluster								
	0	1	2–3	4–9	10–29	30–100	100–299	300–999	1000+
Phase 1 Dishes, 1 hour pointing									
0–0.2	0	0	8	20	0	2	0	0	0
0.2–0.5	54	160	54	0	0	0	0	0	0
0.5–1	568	148	0	0	0	0	0	0	0
> 1	522	10	0	0	0	0	0	0	0
Phase 1 Dishes, 100 hour pointing									
0–0.2	0	0	0	0	8	20	0	2	0
0.2–0.5	0	0	4	162	102	4	0	0	0
0.5–1	2	86	444	182	2	0	0	0	0
> 1	42	370	118	2	0	0	0	0	0
Full SKA dishes, 1 hour pointing									
0–0.2	0	0	0	0	1.6	1.2	0	0.2	0
0.2–0.5	0	0.2	8.6	14.6	3.8	0	0	0	0
0.5–1	1	32	35.8	2.8	0	0	0	0	0
> 1	15.2	35.4	2.6	0	0	0	0	0	0
Full SKA dishes, 100 hour pointing									
0–0.2	0	0	0	0	0	0	2.4	0.4	0.2
0.2–0.5	0	0	0	0	8.6	16.8	1.8	0	0
0.5–1	0	0	0	20.2	49.2	2.2	0	0	0
> 1	0	0.2	10.2	39.4	3.4	0	0	0	0
Full SKA AA, 1 hour pointing									
0–0.2	0	0	0	0	100	250	0	25	0
0.2–0.5	0	0	50	2150	1150	50	0	0	0
0.5–1	25	1175	5550	2175	25	0	0	0	0
> 1	575	4750	1300	25	0	0	0	0	0
Full SKA AA, 100 hour pointing									
0–0.2	0	0	0	0	0	0	150	200	25
0.2–0.5	0	0	0	0	125	2475	800	0	0
0.5–1	0	0	0	350	6925	1675	0	0	0
> 1	0	0	150	4575	1925	0	0	0	0

with a steep decline. With this distribution we have shown to match the observations of nearby clusters. However, one might argue that these nearby clusters may not be representative of whole cluster population. One might imagine that a less centrally peaked flatter distribution, like for example in the Coma cluster, might be more typical. We have shown in section 2.6 above, that the optimum RM-range is between a few and a several  $100 \text{ rad m}^{-2}$ . Such a scenario would therefore lead to an increase of the fraction of sky in our best range. Therefore, the RM-distribution we have chosen is, if anything, rather pessimistic.

We show that with a phase 1 SKA, as defined in Table 1, good stacking experiments should be possible, determining the average magnetic field profile locally and also out to a redshift of about one. The field structure should be measurable for some nearby clusters. If there would be a choice necessary between a deep survey and 100 one hour pointings, one should probably do the deep survey, since it already allows some field structure determination in nearby clusters, and promises to measure RMs for clusters with  $z > 1$ .

With the full SKA AA aperture array, both a shallow 100 one hour pointing survey, and a deep survey promise very interesting results. A shallow 100 times one hour survey should detect RMs

from about  $10^6$  clusters, with complete redshift coverage. A deep 100 h one field survey will allow structure determination in unprecedented detail out to a redshift of one: over 1000 clusters will have more than 100 RM measurements, 25 of which over 1000 RMs. The result of a 100 h deep survey is also shown graphically in Fig. 3 (bottom). To some extent, the two approaches are complementary: the 100 h deep survey would offer a complete RM survey for all structures above  $3 \times 10^{13} M_{\odot}$ , and thereby exclude possible selection biases which could arise if only a fraction of the clusters is detected as in the shallow survey. The shallow survey would be able to detect large scale bias, and also would provide better overall statistics on the cosmological field evolution, if details within the clusters are neglected.

Without phased array feeds on the majority of the dishes, as assumed here, the detection rates remain rather small for the full SKA dish array. However, having similar sensitivity than the aperture array, but coverage at higher frequencies, it would be a valuable complement for high RM regions (cluster centres), where the frequencies accessible to the aperture array would be depolarised. The RM grid density would be similar to the aperture array.

With the deep survey, we could measure the cosmic evolution

**Table 3.** Median maximum rotation measure in any given cluster against redshift for different assumptions about the intrinsic evolution, where  $n$  is the exponent for a systematic change with redshift. The statistical errors are applicable for a 100 hour SKA AA observation. The values in each row have been normalised to the lowest redshift bin.

$n$	$z = 0-0.5$	$z = 0.5-1$	$z = 1-1.5$	$z = 1.5-2$	$z > 2$
1	$1 \pm 0.015$	$0.346 \pm 0.010$	$0.168 \pm 0.012$	$0.066 \pm 0.009$	$0.024 \pm 0.058$
0.5	$1 \pm 0.015$	$0.298 \pm 0.009$	$0.128 \pm 0.009$	$0.047 \pm 0.007$	$0.016 \pm 0.038$
0.2	$1 \pm 0.015$	$0.276 \pm 0.008$	$0.109 \pm 0.007$	$0.039 \pm 0.005$	$0.012 \pm 0.029$
0	$1 \pm 0.015$	$0.259 \pm 0.008$	$0.099 \pm 0.007$	$0.034 \pm 0.005$	$0.010 \pm 0.024$

of the RMs in clusters. If RM is proportional to  $(1+z)^n$ , we could measure  $n$  to an accuracy of  $\Delta n = 0.3$ . In order to determine the evolution of the magnetic field from this, one needs additional information on the electron densities. If we would adopt an accuracy for  $n$  of  $\Delta n = 0.3$ , and assume a similar behaviour and accuracy for the electron densities, to be measured via the Sunyaev-Zel'dovich effect (Sehgal et al. 2005), we would end up with an accuracy for a power law index for the magnetic field ( $B \propto (1+z)^m$ ) of 0.4. This should be regarded as a conservative estimate, since it only takes into account information from the deep survey. Additional information from a shallow survey should improve the accuracy for the low redshift bins. Also, we have only used the information on the maximum RM per cluster. Taking into account the full data, will also improve the statistics.

For a polarised flux limit of  $0.1 \mu\text{Jy}$ , as appropriate for a 100 hour SKA pointing and a SNR of ten, we predict a few 10,000 radio sources per square degree. These sources have a broad redshift distribution, with a median redshift of about one, rising with decreasing flux limit. We can hence expect not only to find the reported numbers of background sources, but also a sizable number of foreground sources, of order a few percent of the background sources, rising of course with cluster redshift. An accurate determination of the foreground RM opens up the possibility to detect a possible small mean cluster RM which would point to a super-cluster scale field connecting the cosmic web. This would be the first detection of such a field.

## 5 CONCLUSIONS

We have modelled the distribution of rotation measures for the SKA. We calculate the average distance between rotation measures to be between 6 arcminutes for a one hour observation with the early SKA and 36 arcseconds for a hundred hour pointing with the full SKA. We expect to find rotation measures mostly up to  $100 \text{ rad m}^{-2}$ , with the cluster centres reaching up to several thousand. The planned SKA mid frequency aperture array (300–1000 MHz) as well as the lowest band of the dish array would be well suited for the great majority of sources. High RM cluster centres would require targeted high frequency follow up observations. We find that current Faraday rotation studies only represent the outskirts of galaxy clusters. The average RM should increase steadily towards the core to reach typically several thousand  $\text{rad m}^{-2}$ .

A phase 1 SKA would already improve the statistics for current stacking experiments considerably, and make this experiment viable out to redshifts  $z > 1$ . The full SKA aperture array would detect over a million clusters with at least one background source each in a shallow 100 hour survey, and allow detailed field structure determination ( $> 1000$  clusters with more than 100 background sources each) with a deep survey. If the cosmological evolution of

the rotation measures is proportional to  $(1+z)^n$ , the SKA would be able to measure  $n$  to an accuracy of 0.3. Compared to the few RMs known for a few nearby clusters today, this will revolutionise our knowledge of rotation measures in galaxy clusters. Provided the electron densities can be measured via the Sunyaev-Zel'dovich effect at high redshift, we can expect to follow the build-up of cosmic magnetism with the SKA.

## ACKNOWLEDGMENTS

This activity was (partly) supported by the European Community Framework Programme 6, Square Kilometre Array Design Studies (SKADS), contract no 011938.

This paper has been typeset from a  $\text{\TeX}/\text{\LaTeX}$  file prepared by the author.

## REFERENCES

- Alexander P., Faulkner, A., 2009, SKA Memo 108, <http://www.skatelescope.org/>
- Bagchi J., Pislar V., Lima Neto G. B., 1998, MNRAS, 296, L23
- Biviano A., Salucci P., 2006, A&A, 452, 75
- Carilli C. L., Taylor G. B., 2002, ARA&A, 40, 319
- Clarke T. E., Kronberg P. P., Böhringer H., 2001, ApJ, 547, L111
- Condon J. J., Cotton W. D., Greisen E. W., Yin Q. F., Perley R. A., Taylor G. B., Broderick J. J., 1998, AJ, 115, 1693
- Feretti L., Dallacasa D., Giovannini G., Tagliani A., 1995, A&A, 302, 680
- Feretti L., Dallacasa D., Govoni F., Giovannini G., Taylor G. B., Klein U., 1999, A&A, 344, 472
- Feretti L., Giovannini G., 2008, in Plionis M., López-Cruz O., Hughes D., eds, Lecture Notes in Physics, Vol. 740, A Panoramic View of Clusters of Galaxies and the Large-Scale Structure, Springer, Dordrecht, p. 143
- Giovannini G., Feretti L., Venturi T., Kim K.-T., Kronberg P. P., 1993, ApJ, 406, 399
- Govoni F., Feretti L., 2004, Int. J. Modern Phys. D, 13, 1549
- Govoni F., Murgia M., Feretti L., Giovannini G., Dolag K., Taylor G. B., 2006, A&A, 460, 425
- Guidetti D., Murgia M., Govoni F., Parma P., Gregorini L., de Ruiter H. R., Cameron R. A., Fanti R., 2008, A&A, 483, 699
- Kaiser C. R., Binney J., 2003, MNRAS, 338, 837
- Kim K.-T., Kronberg P. P., Dewdney P. E., Landecker T. L., 1990, ApJ, 355, 29
- Kim K.-T., Kronberg P. P., Tribble P. C., 1991, ApJ, 379, 80

- Krause M., Alexander P., Bolton R., 2007, in Proceedings of Science, From Planets to Dark Energy: the Modern Radio Universe, POS(MRU)109, <http://pos.sissa.it/>
- Murgia M., Govoni F., Feretti L., Giovannini G., Dallacasa D., Fanti R., Taylor G. B., Dolag K., 2004, *A&A*, 424, 429
- Schilizzi R. T., Alexander P., Cordes J. M., Dewdney P. E., Ekers R. D., Faulkner A. J., Gaensler B. M., Hall P. J., Jonas J. L., Kellermann K. L., 2007, SKA Memo 100, <http://www.skatelescope.org/>
- Sehgal N., Kosowsky A., Holder G., 2005, *ApJ*, 635, 22
- Sheth R. K., Tormen G., 1999, *MNRAS*, 308, 119
- Simard-Normandin M., Kronberg P. P., 1980, *ApJ*, 242, 74
- Taylor A. R., Stil J. M., Grant J. K., Landecker T. L., Kothes R., Reid R. I., Gray A. D., Scott D., Martin P. G., Boothroyd A. I., Joncas G., Lockman F. J., English J., Sajina A., Bond J. R., 2007, *ApJ*, 666, 201
- Taylor G. B., Govoni F., Allen S. W., Fabian A. C., 2001, *MNRAS*, 326, 2
- Tucci M., Martínez-González E., Toffolatti L., González-Nuevo J., de Zotti G., 2003, *New Astron. Rev.*, 47, 1135
- Vogt C., Enßlin T. A., 2005, *A&A*, 434, 67
- Wilman R. J., Miller L., Jarvis M. J., Mauch T., Levrier F., Abdalla F. B., Rawlings S., Klöckner H.-R., Obreschkow D., Olteanu D., Young S., 2008, *MNRAS*, 388, 1335
- Wrobel J., Walker R., 1999, in Taylor G. B., Carilli C. L., Perley R. A., eds, ASP Conf. Ser. Vol. 180, Synthesis Imaging in Radio Astronomy II, Astron. Soc. Pac., San Francisco, p. 171